



# Surface deformation processes in the Carmel Fault based on 17 years of GPS measurements

Gilad Even-Tzur<sup>1</sup> · Joerg Reinking<sup>2</sup>

Received: 6 February 2019 / Accepted: 21 October 2019 / Published online: 16 November 2019  
© Springer-Verlag GmbH Germany, part of Springer Nature 2019

## Abstract

Tectonic activity and crustal deformation in northern Israel are mainly related to the Dead Sea Fault (DSF) and the Carmel–Gilboa Fault System (CGFS). The CGFS is composed of several NW–SE trending faults while the main faults are the Carmel Fault (CF) and Gilboa Fault (GF). The CGFS divides the Sinai Sub-Plate into two tectonic domains. In this study, we geodetically investigate surface deformation processes in the Carmel Fault region. Beside the processing and analysis of GPS measurements, we highlight geodetic aspects in the process of deformation analysis in geodetic monitoring networks. We implement the Extended Free Network Adjustment Constraints solution to calculate the velocities of 24 sites that were measured eight times between 1999 and 2016 using Global Positioning System (GPS). The regional site velocities were estimated with respect to a local datum that was defined by a stable cluster of sites on one side of the fault. We introduced the site velocities into the estimation of surface deformation parameters by using affine transformation also with respect to a local datum. The coordinates of network sites can be transformed to any desired datum by using extended similarity transformation. Examination of the velocity field in relation to a datum defined by points in the Galilee region raises the suggestion that the velocities in the Yizre’el Valley region are due to activities along the GF or similar trending faults on the northern side of the valley which are halted by the Tivon Hills. The best set of deformation parameters, the one which better describes the velocity field, was determined by the second-order Akaike Information Criterion (AICc). The results show significant sinistral deformations of less than 1 mm/year along the Carmel Fault accompanied with extensions and shear strain.

**Keywords** Carmel–Gilboa Fault System · GPS · Velocity field · Extended Free Network · Datum

## 1 Introduction

Tectonic activity and crustal deformation in northern Israel occur mainly on the Dead Sea Fault (DSF) and the Carmel–Gilboa Fault System (CGFS). The DSF is a sinistral transform fault that forms the boundary between the Arabian Plate and the Sinai Sub-Plate mainly on the N–S trending (Fig. 1). The CGFS is composed of several NW–SE trending faults while the main faults are the Carmel Fault (CF) and Gilboa Fault (GF) (Fig. 2). The CGFS divides the Sinai Sub-Plate into two tectonic domains, Galilee-Lebanon in the north and the Israeli backbone terrains in the south

(Ben-Avraham and Ginzburg 1990; Ben-Gai and Ben-Avraham 1995; Hofstetter et al. 1996; Ben-Avraham et al. 2006). This suggests that this shear might define an incipient plate boundary (Sadeh et al. 2012; Wald 2016). The plate south of CGFS is stable, and deformation mainly exists close to the DSF, while north of the fault the deformation is distributed in a wide range (Hofstetter et al. 1996).

The CGFS is a branch of the DSF that starts at the Jordan Valley, goes up to the northern tip of Mount Carmel and extends into the Mediterranean Sea (Fig. 2).

There is no agreement on the exact location of the CGFS. Many authors locate the main fault along the southwestern side of the Yizre’el Valley toward the Fari’a Fault (Nur and Ben-Avraham 1978; Garfunkel 1981; Hofstetter et al. 1996; Rotstein et al. 2004; Fleischer and Gafsou 2005). Others locate the main fault somewhere within the Yizre’el Valley downfaulted structure (Hatzor and Reches 1990; Shaliv 1991; Segev and Rybakov 2011; Segev et al. 2014). Actually, the CGFS is a wide (up to ~ 20 km) deformation zone

✉ Gilad Even-Tzur  
eventzur@technion.ac.il

<sup>1</sup> Division of Mapping and Geo-Information Engineering, Technion - Israel Institute of Technology, Haifa, Israel

<sup>2</sup> Department of Construction and Geoinformation, Jade University of Applied Sciences, Oldenburg, Germany

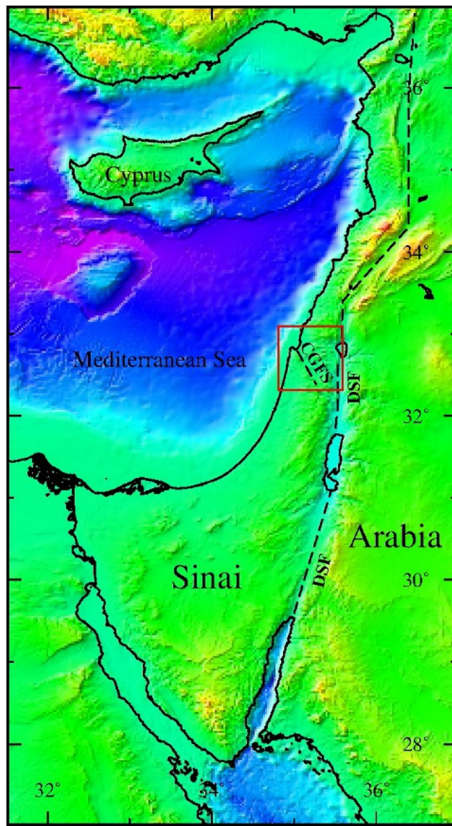


**Fig. 1** Tectonic map of Eastern Mediterranean showing the Sinai and Arabia plates. The black dash line denotes the location of the Dead Sea Fault (DSF). The red box denotes the study area with the Carmel–Gilboa Fault System (CGFS) location

on the valley's southeastern side, which narrows toward the northwest (Mount Carmel). The fault pattern within the Yizre'el Valley is not well known. Rotstein et al. (2004) suggested the presence of major, SW–NE trending, vertical faults with strike-slip components. Others suggested a fault system below the Yizre'el Valley (as presented in Fig. 2), which connects the Gilboa and the Carmel Faults, rather than the Carmel and Fari'a Faults (Segev et al. 2006a, b; Wald et al. 2010; Segev et al. 2014; Wald 2016).

Mount Carmel is an elevated and intensively faulted area that is bordered by the main Carmel Fault on the northeast. The latter is divided into two main segments: A NW–SE-oriented segment that runs from Haifa Bay toward Am-qim Junction (Jalame) and a N–S-oriented fault that runs between Jalame and Yoqneam (Fig. 2). Its continuation southward is the Yoqneam Fault (Segev and Sass 2009). The azimuth of the north segment is about  $145^\circ$ , the same azimuth as the Yoqneam Fault, and the azimuth of the south segment is about  $170^\circ$ . Mount Carmel itself is divided into three blocks that are progressively tectonically elevated to the north by two systems of transverse faults, whose general direction is E–W: the southern and lowest block of Menashe,

the central block of Daliyyat el Carmel and the northern and most elevated block of Haifa. The differences of structural elevations between adjacent blocks vary between 200 and 400 m (Segev and Sass 2014).

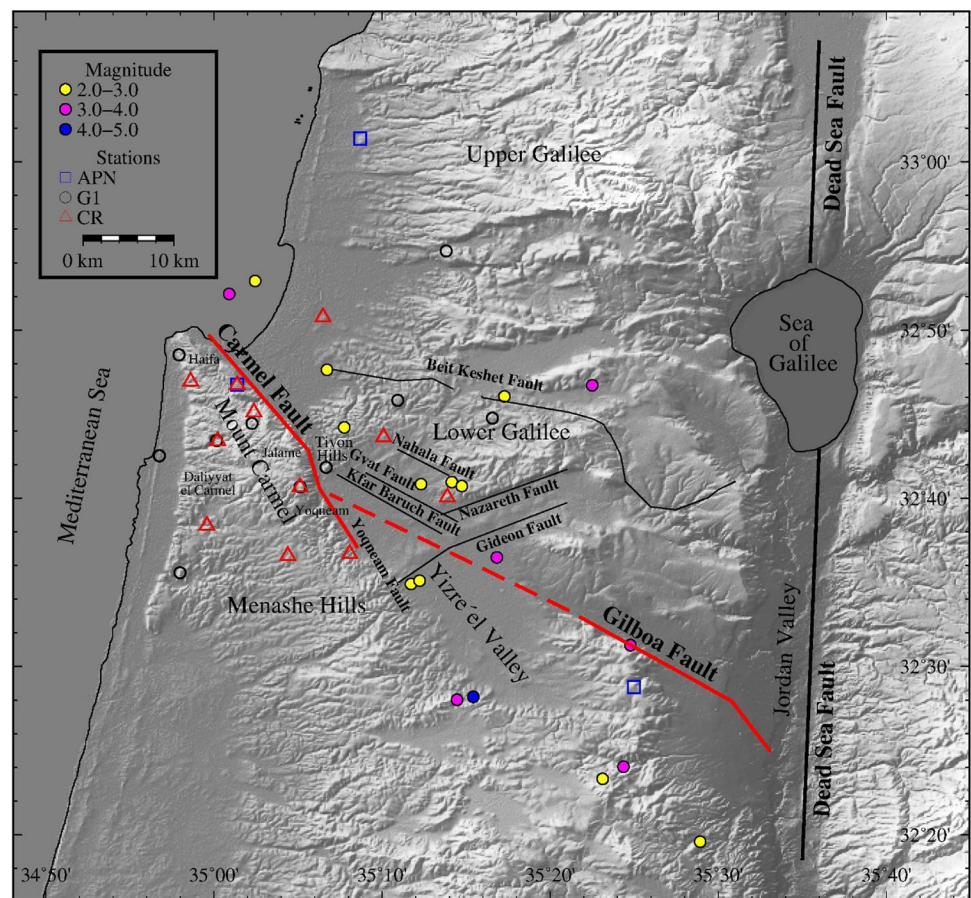
The Carmel Fault is an oblique sinistral–normal fault (e.g., Ben-Gai and Ben-Avraham 1995; Achmon and Ben-Avraham 1997; Sadeh et al. 2012) with estimated horizontal velocities based on geological evidence of less than 1 mm/year (Achmon 1986; Zilberman et al. 2011). In 1984, a moderate earthquake (M5.3) occurred in the study area, and it took place north of the Carmel Fault (Hofstetter et al. 1996), but it did not rupture the surface. Shamir (2007) points out that there is clear evidence of seismic activity along the CGFS between the DSF to the northwest part of Yizre'el Valley, and the activity wanes along the CF in the section between the Tivon Hills and the Mediterranean Sea. The epicenters in the CGFS between the years 1998 and 2017 (during our GPS campaigns) are presented in Fig. 2. A sinistral sense of displacement characterizes some of the earthquake epicenters detected along the CF (Hofstetter et al. 1996).

Previous geodetic studies along the Carmel Fault, based on GPS observations, show controversial displacement rates and senses, ranging from 3.5 mm/year (Agmon 2001) to about 4.5 mm/year dextral (Reinking et al. 2011), through 1 mm/year sinistral (Ostrovsky 2005; Sadeh et al. 2012) to about 2 mm/year sinistral (Shahar and Even-Tzur 2005) and non-significant results (Even-Tzur and Reinking 2013).

Part of the measurement data used in this study served previous studies (Even-Tzur and Reinking 2013; Reinking et al. 2011). The authors of Reinking et al. (2011) stated that their results are in contrast to results from geological and geophysical surveys and must be further investigated. This conclusion results from the use of only five campaigns from which the two earlier campaigns did not include a large number of important sites in the area under investigation. The two later campaigns included all sites cover only a time period of ten years, while the GNSS data from all campaigns were analyzed based on IGS05 reference frame. In Even-Tzur and Reinking (2013), the earlier two campaigns were not included and the GNSS data from the remaining campaigns were reprocessed using IGS08 reference frame that allowed the application of absolute antenna phase center variations. Additionally, GNSS data from two new campaigns are used in this investigation. In total, the observation period covered almost eleven years.

Since the last analysis from Even-Tzur and Reinking (2013), additional four campaigns were conducted and processed, and the useable observation period has been extended to 17 years now. Hence, a new study that uses the results from eight campaigns seems to be advisable. Since this is hitherto the most comprehensive study on this area, it might enable us to establish a more accurate and reliable understanding of the deformation array in the CF region.

**Fig. 2** The digital elevation map of the study area with the location of the main and secondary faults and the location of 24 monitoring network sites. Red lines denote the location of Carmel and Gilboa Faults traces (after Segev and Sass 2009). The red dash line shows the inferred subsurface part of the Gilboa Fault (after Segev et al. 2014; Wald 2016). Thick black lines denote the location of the Dead Sea Fault (DSF). Thin black lines within the Yizre'el Valley denote subsurface faults (after Segev et al. 2014; Wald et al. 2010). Blue squares indicate the location of APN sites. Black circles indicate the location of G1 sites. Red triangles indicate the location of CR sites. Dots denote the locations of earthquakes' epicenter between 1998 and 2017 (The Geophysical Institute of Israel)



In this study, we carry out the Extended Free Network Adjustment Constraints (EFNAC) solution to calculate the horizontal velocities of 24 sites that were measured eight times between 1999 and 2016 using GPS. The result is a velocity field covering the Carmel Fault region. We use affine transformation to extract the horizontal site velocities field into deformation parameters with respect to local geodetic datum defined by some of the network sites. Aspects of datum accuracy, reliability and network sensitivity were taken into account in defining the local datum together with geological considerations. The local datum is taken into account by extended similarity transformation that allows for transforming the coordinates of network sites to any desired datum. The objective of this study is to introduce the actual deformations array in the Carmel Fault region and to highlight geodetic aspects in deformation analysis in geodetic monitoring networks.

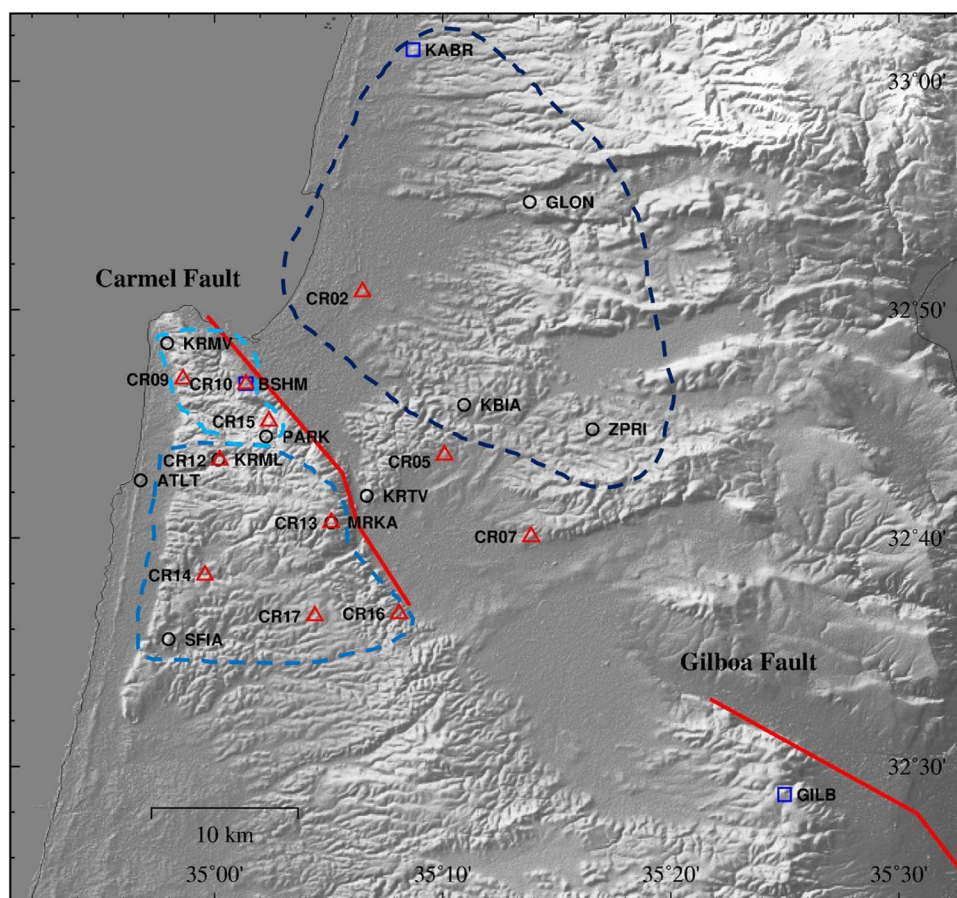
## 2 The GPS network, campaigns and data processing

The CGFS region is covered by a geodetic monitoring network, consisting of 24 sites (Fig. 3) that were measured eight times (1999, 2006, 2009, 2010, 2011, 2012, 2014 and 2016)

by GPS. The network consists of three parts: The Carmel network, the G1 network and the APN network (the APN (Active Permanent Network) is the Israeli network of permanent GNSS sites). The Carmel network (CR) was established in 1989 and is composed of 11 points (Fig. 3, red triangles). The G1 network (Even-Tzur 2006a) was designed and established by the Geological Survey of Israel (GSI) and the Survey of Israel (SOI) in the beginning of the 1990s with the intention of monitoring crustal deformation and serving as the major control network in Israel. Ten G1 sites were measured (Fig. 3, black circles). Three APN sites (Fig. 3, blue squares) are situated in the CGFS region. Additionally, data from another four APN sites (ELAT, RAMO, TELA and KATZ) and three supplementary IGS (International GNSS Service) sites (NICO, ANKR and ZECK) are included in the GPS analysis. Sixteen sites are located southwest to CGFS, while one site is located in the Gilboa, two in Menashe Hills, six in the center part of Mount Carmel and six in the north, and an additional site by the beach. Eight sites are located northeast of CGFS, one in the Tivon Hills and seven in the Galilee region.

The campaigns were measured in six sessions, when all sites were surveyed at least twice in each campaign (Even-Tzur and Reinking 2013). Each session lasted 8 h except in

**Fig. 3** The Carmel–Gilboa Fault System and GPS sites used in this analysis. Blue squares: APN sites. Black circles: G1 sites. Red triangles: CR sites. The dash lines denote groups of points in the network. Blue: Galilee datum. Light Blue: Center and South Carmel. Azure: North Carmel



1999 where every session lasted only 4 h. In 1999 and 2006 campaigns, choke ring antennas were used along with geodetic antennas, since 2009 choke ring antennas were used exclusively.

In total, GPS data from 31 sites were combined into the analysis process. The data for all sites of interest are listed in Table 1. The data from all campaigns were analyzed with the Bernese GNSS Software Version 5.2 (Dach et al. 2015). All campaigns were processed using precise ephemeris, EOPs (Earth Orientation Parameters) and absolute antenna phase center variations with respect to IGS08 (<http://igsceb.jpl.nasa.gov>). We introduced the IGS coordinates from the weekly solution for IGS stations as approximate coordinates to ensure the consistency of all campaign solutions. The datum was defined by loose constraints of the IGS site coordinates. This reduced the influence of possible seasonal variations of site coordinates which are not covered by linear IGS velocities.

### 3 Velocity field estimation

We extract the surface deformation parameters from the horizontal site velocity field, which requires first to estimate the velocity field based on the time series of monitoring

campaigns. The applied method is described briefly below with emphasis on a few issues concerning the datum definition. We start with some basic facts that help to understand the necessity for the application of EFNAC and the Extended S-Transformation.

#### 3.1 The datum problem

Geodetic monitoring networks are used to extract geodynamical quantities such as displacements, velocities and strains, and it is done by using site coordinates. Coordinates are convenient and useful when defined in a proper reference frame: a datum. A datum is defined as a subset of network points, which remain congruent in time at a certain significance level. With a given datum, we may compute positions, displacements, velocities and their variance–covariance matrices.

The positional accuracy of points in a network depends heavily on the spatial distribution of its datum definition points (Papo 2003). It is well known that the positional accuracy of a point is inversely proportional to its distance from the mass center of the datum-points' subset. For GPS networks, the accuracy of the network points is independent of its geometry and the geometrical distribution of

**Table 1** Available GPS data for all campaigns used in this study

Network	Site	Campaign								
		1999	2006	2009	2010	2011	2012	2014	2016	
Carmel	CR02	•	•	•	•	•	•	•	•	
	CR05	•	•	•	•	•	•	•	•	
	CR07	•	•	•	•	•	•	•	•	
	CR09	•	•	•	•	•	•	•	•	
	CR10	•	•	•	•	•	•	•	•	
	CR12	•	•	•	•	•	•	•	•	
	CR13	•	•	•	•	•	•	•	•	
	CR14	•	•	•	•	•	•	•	•	
	CR15	•	•	•	•	•	•	•	•	
	CR16	•	•	•	•	•	•	•	•	
	CR17	•	•	•	•	•	•	•	•	
	G1	ATLT		•	•	•	•	•	•	•
		GLON	•	•	•	•	•	•	•	•
		KBIA		•	•	•	•	•	•	•
		KRML	•	•	•	•	•	•	•	•
		KRMV		•	•	•	•	•	•	•
		KRTV	•	•	•	•	•	•	•	•
MRKA		•	•	•	•	•	•	•	•	
PARK			•	•	•	•	•	•	•	
SFIA		•	•	•	•	•	•	•	•	
ZPRI			•	•	•	•	•	•	•	
APN	BSHM	•		•	•	•	•	•	•	
	ELAT	•	•	•	•	•	•		•	
	GILB	•	•	•	•	•	•			
	KABR	•	•	•	•	•	•	•	•	
	KATZ	•	•	•	•	•	•	•		
	RAMO	•	•	•	•	•			•	
	TELA	•	•	•	•	•			•	
IGS	ANKR	•	•	•	•	•	•	•	•	
	NICO	•		•	•	•	•	•	•	
	ZECK	•	•	•	•	•		•	•	

datum points does not affect the accuracy of the GPS network (Even-Tzur 2000). However, the reliability and sensitivity (the capacity to detect and measure movements and deformations in the area covered by the network) of GPS network depends on geometry. The reliability of a geodetic network depends on the geometrical distribution of the points that define the datum of the network (Even-Tzur 2006b). The sensitivity is invariant to the datum definition, and the geometric location of the network points is extremely important to the network sensitivity (Even-Tzur 2010). In any case, the datum of monitoring network should provide a solid basis for defining the velocities of the points.

Geodetic measurements can, in general, define the inner geometry of the points in the network, but they are incapable of completely determining its datum. In geodetic monitoring networks, the position and velocity of points can be

estimated only if the datum of the network has not been changed between measurement campaigns.

GPS vectors contribute to defining the relative position of points in the network, but they contain only part of the datum definition. They can define datum parameters of orientation and scale but cannot define the network origin. Therefore, the datum defect of a 3D GPS network is three since the definition of origin is missing. The remaining datum parameters, identified with the datum defect of the observational system, are defined by imposing an equal number of linear constraints on the estimated coordinate corrections (Koch 1999).

### 3.2 Strip the datum content from the GPS network

The deformation parameters are estimated based on a time series of monitoring campaigns. The GPS vectors contribute

to the determination of the relative positions of the network points and the datum definition at each epoch. Since we cannot ensure the time stability of the part of the datum defined by the GPS vectors the datum definition may not remain consistent for all epochs.

Possible fluctuations in the GPS orbits between epochs may affect the orientation and scale and impede distinction between the datum components of the measurements and deformation. Even processing of GPS vectors using ephemerides in the same reference frame can only reduce the impact of the GPS vectors' datum contents on the deformation parameters. Without separating the datum components of orientation and scale and deformation factors, the outcome will be a mixture between them.

To preclude the impact of measurement-related datum components in deformation analysis, it is necessary to strip the GPS vectors from their datum definition content. The proper way to combine GPS vector measurements in a network is to filter out their datum definition of scale and orientation and utilize only the sterilized (datumless) quantities in the adjustment. This can be achieved in the adjustment of the network by using Extended Free Network Adjustment Constraints (Papo 1986; Even-Tzur 2011). This mathematical method enables us to solve for parameters that describe the network's global deterministic behavior in addition to the regular adjusted parameters. The conventional datum of the geodetic network in each epoch is defined in its entirety by the preliminary point coordinates and the linear constraints imposed on the corrections to those coordinates.

In this study, in each epoch the GPS vectors are incorporated into a network by utilizing only the sterilized vectors from EFNAC. Based on the datumless sets of coordinates, the variations in the network geometry can be modeled by means of a physical model without the influence of a datum definition inherent in geodetic measurements.

### 3.3 Extended Similarity Transformation—EST

By using Similarity Transformation (S-Transformation), all campaigns can be transformed from one datum to another, avoiding new adjustment computations. It can be done on the coordinates or velocities and on their variance covariance matrices. The known S-Transformation (Baarda 1973) is fitted into an Extended Free Network Adjustment (Even-Tzur 2012; Even-Tzur and Reinking 2013). The resulting EST enables us to filter out of the GPS vectors' datum contents from a coordinate set and to transform the velocities and their variance covariance matrices to a preferable datum. The Bernese GPS software output is a minimal constrained solution of the network points referring to a conventional terrestrial coordinate system and their variance–covariance

matrix. By applying EST to the eight monitoring campaigns, we can filter out the measurement-related datum content of scale and orientations and estimate velocities free of negative effects of those factors.

The EST was used to transform the vector of velocities ( $\dot{x}$ ) and its covariance matrix to a datum that is defined by a group of stable points which were determined by congruency testing (see Even-Tzur and Reinking 2013).

## 4 Deformation analysis

An attempt to apply the infinitely long strike-slip fault model and estimate the left-lateral slip rate and locking-depth on the CF was done by Sadeh et al. (2012). Since the expected slip rate is very low and the distribution of the monitoring points is narrow, especially in the SW side of the network, using a simple dislocation model will not yield reliable results. Therefore, in this study the deformation parameters are determined based on the possibility to deriving them from the changes of the coordinates of a figure placed in a homogeneous strain field. The deformation of a figure can be expressed by an affine transformation of the point coordinates. Deformation of the earth crust is governed by the stress field applied to it. A network of points can represent the structure of the crust. When a stress is applied, it will be expressed by displacement and velocity of the points. When a homogeneous strain field is assumed for a certain area covered by points of the network, a relation between points velocity and deformation parameters can be presented. By this, we transformed the site velocities field into deformation parameters (Brunner 1979; Papo 1985). It is a simple way and easy to adjust that gives us insights into the geodynamic behavior of the study region. The method can be applied on 2D and 3D networks, but since the accuracy of vertical position in GPS networks is low relative to horizontal position, we only deal with 2D networks that is horizontal site velocities.

In two-dimensional analysis of the point velocity field, we are able to compute in total six parameters of an affine transformation: the two parameters of the velocity of the network's barycenter ( $\bar{x}$   $\bar{y}$ ), the rotation parameter ( $r_z$ ) and the deformation rate tensor, which is composed of the scale factors of the two axes ( $d_{xx}^{-1}$   $d_{yy}^{-1}$ ) and the angle between them ( $d_{xy}$ ). The parameters gather in vector  $g$  as:

$$g = \left[ \bar{x} \ \bar{y} \ |r_z \ \left| d_{xx}^{-1} \ d_{yy}^{-1} \right| d_{xy} \right]^T \quad (1)$$

The scale factors present the extensions in the directions of the Cartesian coordinate axes, and the angle between them is the appropriate shearing strain.

We introduce a matrix  $B$  with the following composition:

$$B = \begin{bmatrix} 1 & 0 & -y_1 & x_1 & 0 & y_1 \\ 0 & 1 & x_1 & 0 & y_1 & x_1 \\ \cdot & \cdot & \cdot & \cdot & \cdot & \cdot \\ 0 & 1 & x_u & 0 & y_u & x_u \end{bmatrix} \tag{2}$$

The coordinates  $x_i$ , and  $y_i$  of point  $i$  ( $i = 1, 2, \dots, u$ ) are given in a Cartesian system that is parallel to the reference system and with an origin at the network’s barycenter.

The velocity field of a group of points can be partitioned into a linear model  $Bg$  and a residual vector  $v$ :

$$\dot{x} = Bg + v \tag{3}$$

The velocity vector  $\dot{x}$  has a cofactor matrix  $Q_{\dot{x}}$ , and the vector  $g$  and its cofactor matrix  $Q_g$  are given as:

$$g = (B^T Q_{\dot{x}}^{-1} B)^{-1} B^T Q_{\dot{x}}^{-1} \dot{x} \tag{4}$$

$$Q_g = (B^T Q_{\dot{x}}^{-1} B)^{-1}$$

For a 2D network, at least three non-collinear points are required to define all the elements of vector  $g$ .

It is not obligatory to estimate all the elements of vector  $g$  for a given area represented by a velocity field of some of the network points. It might be possible that only some of the parameters better describe the translation, rotation and deformation array in a part of the area. The structure of  $B$  allows for performing a partial solution, where only part of the six possible parameters are solved with different combinations. Different sets of parameters can be assembled and tested for suitability to the area under study. But, how can we determine what is the best set of parameters, the one which describes best the velocity field. The problem of selecting the “best” set of parameters can be solved using the Akaike’s Information Criterion (AIC) (Akaike 1974). Since, in this study, we deal with a small sample size, the second-order Akaike Information Criterion (AICc) is used instead AIC (Burnham and Anderson 2002).

### 5 Results

Eight campaigns of horizontal coordinates and their variance–covariance matrices, observed over a period of 17 years, were obtained from the GPS analysis. The data were used to derive site velocities by EFNAC.

First, we introduced the velocity field related to the Galilee datum. Five points (KABR, GLON, CR02, KBIA and ZPRI) in the north part of the monitoring network were selected to define the datum (see Fig. 3). The datum points are located on one side of the fault and may introduce a homogeneous geological region. These points are located sufficiently far from the DSF, where the contribution of the

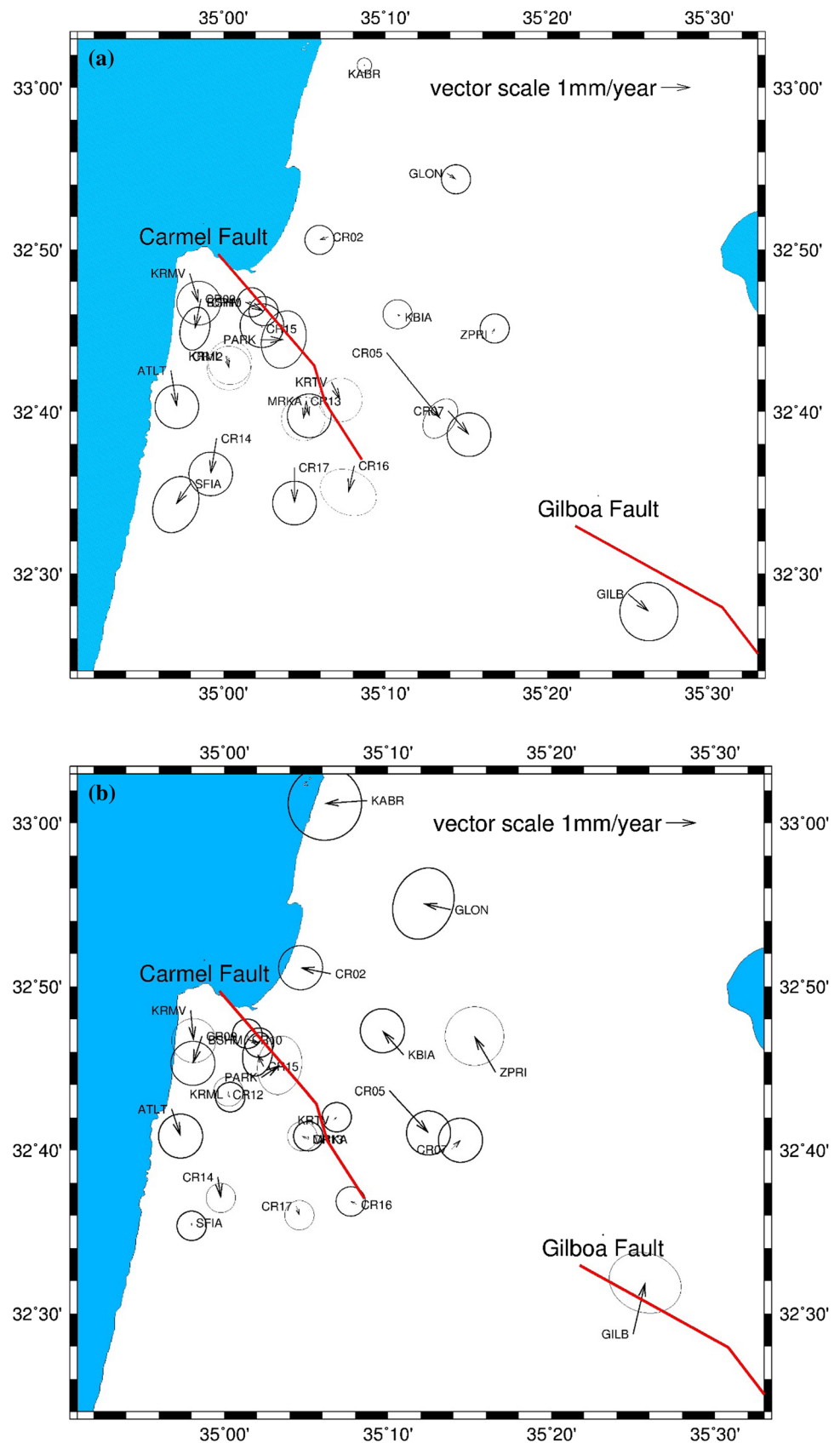
ground displacement due to slip along the DSF is expected to be very small. Congruency testing was performed to determine the stability of the datum points (Koch 1999). The calculated value  $\omega = (\dot{x}^T Q_{\dot{x}}^{-1} \dot{x})/h$  is tested against  $F(\alpha;h;r)$ , which is determined based on the Fisher distribution. With the chosen significance level  $\alpha = 5\%$ , the degrees of freedom  $r = \infty$  (since the degrees of freedom resulting from the Bernese GPS Software was enormous) and the rank of the cofactor matrix of datum points velocities ( $Q_{\dot{x}}$ ),  $h = 6$ ,  $F(0.05;6;\infty) = 2.10$  was obtained. The value of  $\omega = 0.17$  was obtained. Because  $\omega < F$ , the five points define a stable datum, which means that there is no significant movement between the datum points. Figure 4a depicts the velocity vectors and their 95% confidence ellipses across the CGFS when compared with the Galilee datum points. The velocity field clearly shows significant velocities in the region under investigation. Points CR05 and CR07 which are ostensibly located on the northeast side of CGFS show movement similar in direction to points on the southwest side of the faults. The velocity of point CR05 is anomalous with respect to other sites.

Points which are close to CF, including points CR12 and KRML, show stability relative to the datum points. Points on the west side of the network (KRMV, CR09, ATLT and CR14) show significant movement to the south, indicating a left-lateral sense of slip along the CF of about 1 mm/year. Those points are located on the western slopes of Mount Carmel except ATLT, which is located at the sea sandstone (Kurkar) ridge by the beach.

The point MRKA and the nearby point CR13 show no significant velocities and neither does KRTV, although located close to them on the other side of the fault, relative to the datum sites. Points CR07 and CR16, which are located at the edge of the Yizre’el Valley on both sides, express the same velocity in the same direction. The velocity of GILB, which is expected to be affected the most by ground displacement due to slip along the DSF, shows velocity that is appropriate to a sinistral movement along the GF.

An additional expression of the velocity field in the region can be obtained when points located on the south and center part of Mount Carmel are used to define the datum (Fig. 4b). Two sites on the southern block of the Menashe Hills (CR16 and CR17) and five points on the central block of Daliyyat el Carmel (CR12, KRML, CR13, MRKA and SFIA) define the Carmel datum. With a 5% level of significance, those points define a stable datum, since for those datum points  $\omega = (\dot{x}^T Q_{\dot{x}}^{-1} \dot{x})/h = 0.04$  which is less than  $F(0.05;6;\infty) = 2.10$ . The five points which are located in the Galilee region significantly show sinistral movement relative to the Carmel Datum. Point CR05 shows anomalous velocity in direction opposite to other points which are located in the Galilee region. This may reflect a local site effect only since extensive construction activities were carried out near that

**Fig. 4** The velocity vectors and their 95% confidence ellipses across the Carmel–Gilboa Fault System (CGFS) **a** relative to the Galilee datum defined by points KABR, GLON, CR02, KBIA and ZPRI **b** relative to the Carmel datum defined by points CR16, CR17, SFIA, CR12, KRML, CR13 and MRKA. Analysis is based on eight measuring campaigns carried out between 1999 and 2016. Red lines denote the geological fault traces. Point names in blue square are points in the datum definition





site during the observation period. Points CR07 and KRTV, which are located on the northeast side of the fault, show no movement and neither do points along the north segment of the CF, which are located on the southwest side of the fault.

Deformation parameters from the horizontal site velocities field are extracted referring to the Galilee Datum. The network points in the Carmel region were divided into three groups: (a) Carmel North—including six points: KRMV, CR09, BSHM, CR10, CR15 and PARK, all located on the north part of Mount Carmel; (b) Carmel Center and South—including 6 points: KRML, CR12, MRKA, CR13, CR14 and SFIA, all located on the center part of the mountain, and points CR16 and CR17, located on the Menashe Hills; (b\*) Carmel Center and South, which additionally includes KRTV and CR07; (c) Carmel—includes all points of Carmel North, Center, South and ATLT (see Fig. 3). In order to define the best set of parameters, the one which describes best the velocity field, various sets of parameters

parameters that compose each set are presented in Table 2. In all sets, the two parameters of the velocity of the network’s barycenter were used with additional parameters, such as rotation, scale and obliquity. In some sets, we used one common scale factor instead of a different factor for each axis. Then, the best model was determined by AICc. The AICc penalizes for the addition of parameters and thus selects a model that fits well but has a minimum number of parameters. A good mathematical model is one that has the smallest AICc score. As an example, the AICc score of the 12 models for the Carmel tested area, case (c), is seen in Table 2. The best set is number 8, with a score of 139.2. The worst one is number 6 with a score of 152.6. The best set of parameters and their standard deviations for each tested area is presented in Table 3. With a 5% level of significance, the velocity of the subnetworks’ barycenter, scales and angle between the axes is significant.

Comparing the three models, it can be seen that the

**Table 2** The deformation parameters that compose each set and its AICc score for the Carmel tested area. In all sets, the two parameters of the velocity of the network’s barycenter ( $\bar{x}$ ,  $\bar{y}$ ) were used with additional parameters as rotation ( $r_z$ ), scale factor for each axis ( $d_{xx}^{-1}$ ,  $d_{yy}^{-1}$ ), common scale ( $d_{xy}^{-1}$ ) and obliquity ( $d_{xy}$ ). The chosen model is the one with the minimum score

Model	Deformation parameters							AICc score
	$\bar{x}$	$\bar{y}$	$r_z$	$d_{xx}^{-1}$	$d_{yy}^{-1}$	$d_{xy}^{-1}$	$d_{xy}$	
1	✓	✓						149.6
2	✓	✓	✓					148.6
3	✓	✓					✓	142.9
4	✓	✓				✓		150.2
5	✓	✓	✓			✓		149.0
6	✓	✓		✓	✓			152.6
7	✓	✓	✓				✓	145.2
8	✓	✓				✓	✓	139.2
9	✓	✓	✓	✓	✓			151.8
10	✓	✓		✓	✓		✓	142.0
11	✓	✓	✓			✓	✓	141.9
12	✓	✓	✓	✓	✓		✓	145.0

were composed. The six parameters of vector  $g$  (Eq. 1) were used to create 12 sets of parameters. The deformation

deformation model of the north part of Carmel is characterized by a moderate velocity of the network’s barycenter,

**Table 3** Surface deformation parameters and their standard deviations which best describe the velocity field in (a) Carmel North, defined by points KRMV, CR09, BSHM, CR10, CR15 and PARK; (b) Carmel Center and South, defined by points KRML, CR12,

MRKA, CR13, CR14, SFIA, CR16 and CR17; (b\*) same as Carmel Center and South but with additional points KRTV and CR07; (c) Carmel, defined by Carmel North, Center and South and ATLT. The best model was determined by AICc among 12 optional models

Tested area	Deformation parameters						
	$\bar{x}$ (mm/year)	$\bar{y}$ (mm/year)	$r_z \cdot 10^{-8}$ (rad/year)	$d_{xx}^{-1} \cdot 10^{-8}$ (1/year)	$d_{yy}^{-1} \cdot 10^{-8}$ (1/year)	$d_{xy}^{-1} \cdot 10^{-8}$ (1/year)	$d_{xy} \cdot 10^{-8}$ (rad/year)
(a) Carmel North	$-0.49 \pm 0.17$	$0.27 \pm 0.17$	–	–	–	$12.5 \pm 3.3$	$18.4 \pm 3.3$
(b) Carmel Center and South	$-0.81 \pm 0.24$	$0.10 \pm 0.21$	–	–	–	$3.4 \pm 1.2$	–
(b*) Carmel Center and South with KRTV and CR07	$-0.79 \pm 0.22$	$0.22 \pm 0.19$	–	–	–	$3.8 \pm 1.0$	–
(c) Carmel	$-0.63 \pm 0.19$	$0.21 \pm 0.16$	–	–	–	$3.7 \pm 0.9$	$4.2 \pm 0.6$

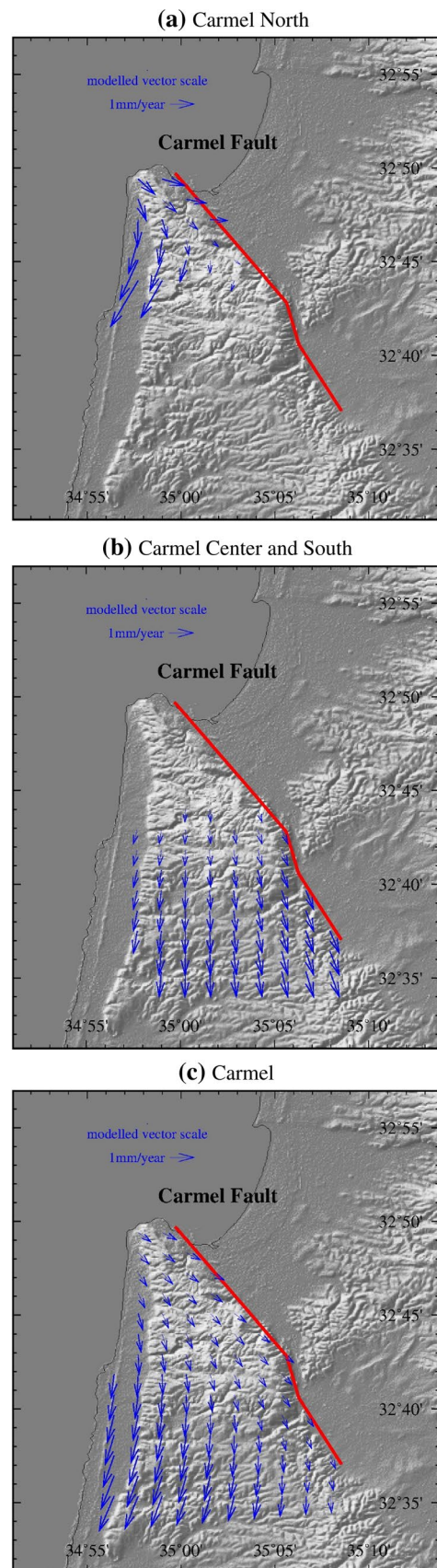
**Fig. 5** Modeled velocity field calculated based on the surface deformation parameters presented in Table 3 for **a** Carmel North, **b** Carmel Center and South, **c** Carmel. The modeled velocity field of **a** reflects the activity along the north segment of the CF. The modeled velocity field of **b** reflects the activity along the south segment of the CF and Yoqneam Fault

$0.56 \pm 0.17$  mm/year in the azimuth of  $150^\circ$ . The scale factor is the same for both axes with a relative high value, and so is the angle between the axes. The model describing the deformation of the Carmel center and south shows velocity of  $0.82 \pm 0.24$  mm/year in the azimuth of  $173^\circ$  of the network's barycenter with a moderate scale factor for both axes. The model which describes the deformation in all of the Carmel area shows velocity of  $0.66 \pm 0.19$  mm/year in the azimuth of  $162^\circ$  of the network's barycenter with a moderate scale factor for both axes and the angle between them.

Illustrations of the models are presented in Fig. 5; it shows the resulting gridded velocity field for the Carmel area. The velocity field of the north part of Carmel should reflect the activity along the north segment of the CF and the velocity field of the Carmel center and south reflect the activity along the south segment of the CF and Yoqneam Fault relative to the Galilee datum. The velocity of the network's barycenter of the north part of Carmel is parallel to the north segment of the CF and the velocity of the Carmel center and south is parallel to the south segment.

## 6 Discussion and conclusions

The creation of an accurate and reliable velocity field is based on eight monitoring campaigns over a long period of 17 years, 8-h measurement sessions, measuring each network point at least twice in each campaign and using sophisticated mathematical tools. The regional site velocities were estimated with respect to a local datum that was defined by a stable cluster of sites on one side of the fault by means of EFNAC. The velocity field clearly shows significant velocities in the study area. Points CR05 and CR07 show unexpected velocities, velocities which are apparently not compatible with the location of CGFS as shown in Fig. 2. Indeed, the velocity of point CR05 is anomalous, but it has the same direction as CR07 but with a larger velocity. The possibility of gross errors in the time series of the CR05 location must be examined. There are many methods and techniques for gross errors detection in time series of data, mainly based on statistical tests and robust methods. If an observation with gross error is detected, it must be eliminated to prevent it from distorting the estimation of velocity.



An examination of the time series of CR05 location does not raise a suspicion of a gross error in one of the monitoring campaigns. The unusual velocities of CR05 and CR07 can be explained by slope failure or rockslide, but looking at the Geological Survey of Israel landslide hazard map (Katz and Almog 2006), it is noticed that the area is characterized by low sensitivity for landslides. Rotstein et al. (2004) suggest that the Nahalal Fault has a strike-slip component and it appears to be an important active fault in the northwest boundary of Yizre'el Valley (see Fig. 2). We would suggest that the significant velocity of CR07 and CR05 is the result of a deformation related to the fault. However, the unusual velocity of CR05 can be caused additionally by local site effects. Therefore, we should consider establishing a dense monitoring network in the area of CR05 and CR07. It will give us the option to estimate if the anomalous velocity of CR05 is due to local behavior or it is indeed a significant behavior of the entire area.

The pair of adjacent points MRKA and CR13 on the south side of CF and KRTV on the north side is close to each other (a distance of about 3 km) and shows no significant velocities. Points CR07 and CR16, which are located on both sides of the Yizre'el Valley as well as on both sides of the N–S-oriented south segment of CF, show the same velocities in the same direction relative to the Galilee datum. Relative to the Carmel datum CR07 as well as KRTV show insignificant velocity. Those points which are in the north side of CF show no velocity relative to the Carmel datum which is located on the south side of CF. This may indicate that the south segment of CF is not active, a conclusion that supports other studies of Shaliv (1991), Segev and Rybakov (2011) and Segev et al. (2014).

The area represented by KRTV (Tivon Hills) and MRKA (Carmel) is the meeting point of CF and GF (see Fig. 2) (Segev and Sass 2009; Wald 2016). The insignificant velocities of those two points relative to the Galilee datum and the significant velocities of CR16 and CR07 may indicate that the southern segment of CF is not active. One can suggest that the velocities in the Yizre'el Valley region are due to activities along the GF or similar trending faults, which are halted by the Tivon Hills. This hypothesis can be reinforced by Shamir (2007), who points out that seismic activity wanes along the CF in the Tivon Hills region.

Since it is doubtful whether the infinitely long strike-slip fault model can be applied in the research area, we used affine transformation to extract the horizontal site velocities field into surface deformation parameters. The Mount Carmel region was divided into two areas, Carmel North and Carmel Center and South, and deformation parameters were estimated for each area. The use of AICc allowed us to choose the best model among several. The best model is defined as the one that better describes the velocity field.

The values of velocities and deformation parameters in the research area are very small as can be seen in Table 3, yet the values are significant at a 95% confidence level. The velocity components in the y directions of the subnetworks' barycenter are small, and their standard deviations are larger than the corresponding value. However, the main velocity directions are along the x axis and these values are significant. Therefore, the overall velocity of the subnetworks' barycenter is significant.

While the deformation structure of Carmel north is composed of moderate velocity ( $0.56 \pm 0.17$  mm/year), large extension ( $1.25 \times 10^{-7} \pm 3.3 \times 10^{-8}$  1/year) and shear strain ( $1.84 \times 10^{-7} \pm 3.3 \times 10^{-8}$  rad/year), the deformation structure of Carmel Center shows higher velocity ( $0.82 \pm 0.24$  mm/year) with small extensions ( $3.4 \times 10^{-8} \pm 1.2 \times 10^{-8}$  1/year) with no shear strain.

When we examine the velocities and deformations in the entire Carmel region, we obtain a result that effectively combines the two partial results of the northern and center Carmel (velocity of  $0.66 \pm 0.19$  mm/year, extension of  $3.2 \times 10^{-8} \pm 0.9 \times 10^{-8}$  1/year and shear strain of  $4.2 \times 10^{-8} \pm 0.6 \times 10^{-8}$  rad/year). It is interesting to note that rigid body rotation is not part of the fabric of velocities and deformation in the Carmel area. In conclusion, the results show deformations of less than 1 mm/year sinistral along the Carmel Fault accompanied by extensions and shear strain.

We also examined the option that points KRTV and CR07 are part of the Carmel Center and south group of points and defined the best set of parameters that better describe the velocity field of those points. The same set of parameters with very similar values were obtained with and without those two points (see Table 1 option (b\*)). This may indicate that the array of deformations in the Tivon Hills and in the northeast part of the Yizre'el Valley is similar to that determined for the center part of the Carmel region. We suggest that today the fault line in this area runs along the southern downs of the Lower Galilee, adjacent to the Yizre'el Valley.

It lies in the nature of this planet that no velocity of a site is affected by only one single fault. Commonly, a deformation field is influenced by a system of major and minor fault. Hence, one can expect that the velocities in the study area are a combination of deformation related both to the CGFS and the DSF. The network points are located far from the DSF, except GILB (thus, it does not participate in the deformation analysis), and if an effect of deformation along the DSF on the velocities exist, it is assumed to be small. No attempt was done to evaluate the impact of the DSF on the velocity field, but to present the actual velocities and deformations in the Carmel Fault region. Elimination the impact caused by the DSF in the study area requires knowledge about its nature. Any model used to evaluate the deformation

caused by the DSF may contribute biases to the deformation analysis in the research area which is something we want to avoid.

**Acknowledgements** Most of the measurements that were used in this study were obtained during summer camps carried out by undergraduate and graduate students from the Division of Mapping and Geo-Information Engineering, Technion, Israel; and the Department of Construction and Geoinformation, Jade University of Applied Sciences, Germany, under the supervision of Hillrich Smit-Philipp. We greatly appreciate their significant contribution.

**Author contributions** GET and JR designed and performed the research. JR analyzed the GPS data, and GET takes responsibility for the integrity of the data and data analysis. GET wrote the paper, and JR revised it critically and approved the final version.

**Data availability** G.E.T. and J.R. have full access to the GPS data used in the study and are available upon reasonable request. All other data, models, or code generated or used during the study are available from the corresponding author by request.

## References

- Achmon M (1986) The Carmel border fault between Yoqneam and Nesher. Ms. C. Thesis, The Hebrew University of Jerusalem (in Hebrew, with English abstract)
- Achmon M, Ben-Avraham Z (1997) The deep structure of the Carmel fault zone, northern Israel, from gravity field analysis. *Tectonics* 16(3):563–569
- Agmon E (2001) Algorithm for the analysis of deformation monitoring networks. M.Sc. thesis, Technion, Israel Institute of Technology, Haifa (**in Hebrew, with English abstract**)
- Akaike H (1974) A new look at the statistical model identification. *IEEE Trans Autom Control* 19(6):716–723
- Baarda W (1973) S-Transformation and criterion matrices. Netherlands Geodetic Commission, Publication on Geodesy, New Series, vol 5, no 1
- Ben-Avraham Z, Ginzburg A (1990) Displaced terranes and crustal evolution of the Levant and the eastern Mediterranean. *Tectonics* 9(4):613–622
- Ben-Avraham Z, Schattner U, Lazar M, Hall JK, Ben-Gai Y, Neev D, Reshef M (2006) Segmentation of the Levant continental margin, eastern Mediterranean. *Tectonics* 25:TC5002. <https://doi.org/10.1029/2005tc001824>
- Ben-Gai Y, Ben-Avraham Z (1995) Tectonic processes in offshore northern Israel and the evolution of the Carmel structure. *Mar Petrol Geol* 12:533–548
- Brunner FK (1979) On the analysis of geodetic networks for the determination of the incremental tensor. *Surv Rev* 25:56–67
- Burnham KP, Anderson DR (2002) Model selection and multimodel inference: a practical-theoretic approach, 2nd edn. Springer, New York, p 496
- Dach R, Lutz S, Walser P, Fridez P (2015) Bernese GNSS software version 5.2. Astronomical Institute, University Bern. <http://www.bernese.unibe.ch/docs/DOCU52.pdf>
- Even-Tzur G (2000) Datum definition for GPS networks. *Surv Rev* 35(277):475–486
- Even-Tzur G (2006a) Designing the configuration of the geodetic–geodynamic network in Israel. *Geodetic deformation monitoring: from geophysical to engineering roles*. In: Sanso F, Gil AJ (eds) International association of geodesy symposia, vol 131. Springer, New York, pp 146–151
- Even-Tzur G (2006b) Datum definition and its influence on the reliability of geodetic networks. *Z Vermess* 131(2):87–95
- Even-Tzur G (2010) More on sensitivity of a geodetic monitoring network. *J Appl Geodesy* 4(1):55–59
- Even-Tzur G (2011) Deformation analysis by means of extended free network adjustment constraints. *J Surv Eng* 137:47–52
- Even-Tzur G (2012) Extended S-transformation as a tool for deformation analysis. *Surv Rev* 44:315–318
- Even-Tzur G, Reinking J (2013) Velocity field across the Carmel fault calculated by extended free network adjustment constraints. *J Appl Geodesy* 7(2):75–82
- Fleischer L, Gafsou R (2005) Structural map on top Judea group. In: Hall JK, Krashennikov VA, Hirsch F, Benjamini C, Flexer A (eds) Geological framework of the Levant, plates (plate V). Historical Productions-Hall, Jerusalem
- Garfunkel Z (1981) Internal structure of the Dead Sea leaky transform (rift) in relation to plate kinematics. *Tectonophysics* 80:81–108
- Hatzor Y, Reches Z (1990) Structure and paleostresses in the Gilboa’ region, western margins of the central Dead Sea rift. *Tectonophysics* 180:87–100
- Hofstetter A, van Eck T, Shapira A (1996) Seismic activity along the fault branches of the Dead Sea–Jordan transform: the Carmel–Tirtza fault system. *Tectonophysics* 267:317–330
- Katz O, Almog E (2006) National hazard map for earthquake induced landslides in Israel; Northern sheet, scale 1: 200,000. Israel geological survey Rep. GSI/38/2006, 16 pp. (**in Hebrew**)
- Koch KR (1999) Parameter estimation and hypothesis testing in linear models, 2nd edn. Springer, Berlin
- Nur A, Ben-Avraham Z (1978) The eastern mediterranean and the Levant: tectonics of continental collision. *Tectonophysics* 46(3–4):297–311
- Ostrovsky E (2005) The G1 geodetic geodynamic network: results of the G1 GPS surveying campaigns in 1996/1997 and 2001/2002. Technical project report, Survey of Israel
- Papo HB (1985) Deformation analysis by close-range photogrammetry. *Photogramm Eng Remote Sens* 51:1561–1567
- Papo HB (1986) Extended free net adjustment constraints. NOAA technical report NOS 119 NGS 37, 16
- Papo HB (2003) Datum accuracy and its dependence on network geometry. In: Grafarend EW, Krumm FW, Schwarze VS (eds) *Geodesy—the challenge of the 3rd millennium*. Springer, Berlin, pp 379–386
- Reinking J, Smit-Philipp H, Even-Tzur G (2011) Surface deformation along the Carmel fault system, Israel. *J Geodyn* 52(3–4):321–331
- Rotstein Y, Shaliv G, Rybakov M (2004) Active tectonics of the Yizre’el valley, Israel, using high-resolution seismic reflection data. *Tectonophysics* 382:31–50
- Sadeh M, Hamiel Y, Ziv A, Bock Y, Fang P, Wdowinski S (2012) Crustal deformation along the Dead Sea Transform and the Carmel Fault inferred from 12 years of GPS measurements. *J Geophys Res* 117:B08410. <https://doi.org/10.1029/2012JB009241>
- Segev A, Rybakov M (2011) History of faulting and magmatism in the Galilee (Israel) and across the Levant continental margin inferred from potential field data. *J Geodyn* 51(4):264–284
- Segev A, Sass E (2009) The geology of the Carmel region; Albian–Turonian volcano–sedimentary cycles on the north-western edge of the Arabian platform. Geological Survey of Israel Report GSI/7/2009 (**in Hebrew with English abstract**)
- Segev A, Sass E (2014) Geology of Mount Carmel—completion of the Haifa region. Israel geological survey report GSI/18/2014, 64 pp. (**in Hebrew with English abstract**)
- Segev A, Reznikov M, Lyakhovskiy V, Rybakov M, Shaliv G, Schattner U (2006) The Carmel–Gilboa fracture system: study of the Emeq Yizreel subsurface. Israel geological survey report GSI/36/2006, 45 pp. (**in Hebrew with English abstract**)

- Segev A, Rybakov M, Lyakhovsky V, Hofstetter A, Tibor G, Goldshmidt V, Ben-Avraham Z (2006b) The structure, isostasy and gravity field of the Levant continental margin and the southeast Mediterranean area. *Tectonophysics* 425:137–157
- Segev A, Lyakhovsky V, Weinberger R (2014) Continental transform–rift interaction adjacent to a continental margin: the Levant case study. *Earth Sci Rev* 139:83–103
- Shahar L, Even-Tzur G (2005) Deformation monitoring in the Northern Israel between the years 1996 and 2002. Geodetic deformation monitoring: from geophysical to engineering roles. In: Sanso F, Gil AJ (eds) *International association of geodesy symposia*, vol 131. Springer, New York, pp 146–151
- Shaliv G (1991) Stages in the tectonic and volcanic history of the Neogene basin in the Lower Galilee and the valleys. Report GSI/11, 91, p 94
- Shamir G (2007) Earthquake epicenter distribution and mechanisms in northern Israel. Israel geological survey report GSI/16/2007, 40 pp. **(in Hebrew with English abstract)**
- Wald R (2016) Interpretation of the lower (southern) Galilee tectonic evolution from Oligocene truncation to Miocene Pliocene deformation using geological and geophysical subsurface data. Israel geological survey report GSI/15/2016, 216 pp. **(in Hebrew with English abstract)**
- Wald R, Schattner U, Segev A, Ben-Avraham Z (2010) The Yizre'el Valley—structure and tectonics. Israel geological survey report GSI/36/2010, 216 pp. **(in Hebrew with English abstract)**
- Zilberman E, Greenbaum N, Nahmias Y, Porat N (2011) The evolution of the Northern Shutter Ridge, Mt. Carmel, and its implications on the tectonic activity along the Yagur fault. Israel geological survey report GSI/14/2011, 25 p